RSC Advances

PAPER

View Article Online
View Journal | View Issue

Cite this: *RSC Adv.*, 2016, **6**, 60101

A thermodynamic investigation of the $LiBH_4$–$NaBH_4$ system†

Erika M. Dematteis,[ab] Elsa Roedern,[b] Eugenio R. Pinatel,[a] Marta Corno,[a] Torben R. Jensen[b] and Marcello Baricco*[a]

Received 11th April 2016
Accepted 16th June 2016

DOI: 10.1039/c6ra09301a

www.rsc.org/advances

The $LiBH_4$–$NaBH_4$ pseudo-binary system has been investigated by X-ray diffraction, temperature-programmed photographic analysis, and differential scanning calorimetry, in order to establish the phase diagram. The polymorphic orthorhombic-to-hexagonal phase transition of $LiBH_4$ was observed at 94 °C in samples containing $NaBH_4$, *i.e.* 15 °C lower than for pure $LiBH_4$, which indicates the dissolution of sodium into $LiBH_4$. The formation of solid solutions was confirmed by powder X-ray diffraction measurements performed as a function of temperature. A new eutectic composition between $Li_{0.65}Na_{0.35}BH_4$ and $Li_{0.70}Na_{0.30}BH_4$, with a melting temperature of 216 °C, is observed. *Ab initio* calculations have been performed to establish the relative stabilities of the pure compounds in orthorhombic, hexagonal and cubic structures. The obtained experimental and calculated data were compared with available literature values and they were used for a thermodynamic assessment of the $LiBH_4$–$NaBH_4$ system by the calphad method. The enthalpy of mixing for solid and liquid solutions has been estimated on the basis of experimental data.

Introduction

Any strategy to address climate change must involve the phasing-out of fossil fuels. However, renewable energy sources fluctuate geographically and over time. It is therefore important to design a system that allows storage of electrical or thermal energy and utilisation at another place or time. Hydrogen is considered as a potential future energy carrier for mobile and large-scale stationary applications, but it requires an efficient storage strategy.[1] Recent research has been focused on solid-state hydrogen storage materials, which allow the storage of hydrogen at low pressures. In particular, complex hydrides have been considered and, among them, metal borohydrides are interesting compounds owing to their high gravimetric hydrogen content.[2–5] In the context of batteries, complex hydrides have also been investigated as possible solid-state electrolytes.[6–8]

Owing to their low temperature of melting, eutectic mixtures of complex hydrides can easily be infiltrated into porous scaffolds.[9,10] In this way, the kinetics and reversibility of hydrogen sorption reactions can be improved, because nanosized particles are preserved during cycling. Moreover, low melting mixtures of complex hydrides have been studied recently as ionic liquids, aiming to provide fast and convenient re-fuelling of hydrogen in fuel cell vehicles.[11,12] The use of eutectic mixtures is strongly related to the stability of the liquid phase, therefore the characterization of their thermodynamic properties is of fundamental importance.[13]

Mixtures of metal borohydrides often show eutectic melting, *e.g.* the mixture of lithium and potassium borohydride, $0.72LiBH_4$–$0.28KBH_4$, with a melting point as low as T_e = 105 °C.[14–16] For the $LiBH_4$–$NaBH_4$ system, an eutectic composition $0.62LiBH_4$–$0.38NaBH_4$, melting at 220 °C, was reported more than 40 years ago.[17,18] A partial pseudo-binary $LiBH_4$–$NaBH_4$ phase diagram was proposed by Adams in 1961, describing the system as eutectic and reporting experimental liquidus points in the $LiBH_4$-rich mixtures, however without detailing the experimental method used for their determination.[17] In 1971, Semenenko *et al.* conducted a study of the pseudo-binary phase diagram by coupling thermographic and X-ray investigation on annealed samples. The system was described without any eutectic point, but it was characterized by the formation of solid solutions with a miscibility gap and a minimum melting temperature at the same composition previously proposed by Adams as eutectic ($0.62LiBH_4$–$0.38NaBH_4$).[18] It is worth noting that solid solutions of metal borohydrides have recently received attention, especially those of $LiBH_4$ with alkali metal halides, since it was reported that $LiBH_4$–LiI shows fast-ion conduction, owing to the stabilization of the hexagonal HT-structure of $LiBH_4$ at room temperature.[19–27]

[a]*Department of Chemistry and Inter-Departmental Center Nanostructured Interfaces and Surfaces (NIS), University of Turin, Via Pietro Giuria 7, 10125 Torino, Italy. E-mail: marcello.baricco@unito.it; Fax: +39 0116707856; Tel: +39 011 6707569*

[b]*Department of Chemistry, Center for Materials Crystallography (CMC) and Interdisciplinary Nanoscience Center (iNANO) Aarhus University, Langelandsgade 140, DK-8000 Aarhus C, Denmark*

† Electronic supplementary information (ESI) available: Additional table with all temperatures and peaks area obtained from DSC measurements. All TPPA, DSC, HT-PXD and SR-PXD data collected. See DOI: 10.1039/c6ra09301a

Since the reported phase diagrams are not coherent and the experimental points are not fully described, further investigations are necessary. Therefore, in the present study, a systematic investigation of the thermodynamics of the $LiBH_4$–$NaBH_4$ system has been carried out. The formation of solid solutions at both room temperature and elevated temperature has been evidenced. The pseudo-binary phase diagram has been established, combining various experimental techniques. Literature, experimental and *ab initio* data have been used for a thermodynamic assessment of the system using the calphad approach.[28]

Experimental

Sample preparation

The purity of lithium borohydride ($LiBH_4$) was >99%, as determined by ICP analysis (Table S1†). Sodium borohydride ($NaBH_4$) was purchased from Sigma-Aldrich, purity 99.99%. The samples were prepared by mechanochemical treatment, *i.e.* ball milling (BM) of the reactants in a Fritsch Pulverisette 6 planetary mill under argon atmosphere in 80 mL tungsten carbide (WC) containers and with WC balls (o.d. 6 mm). $LiBH_4$ and $NaBH_4$ were mixed in various molar rations, corresponding to balls-to-sample mass ratio of 30 : 1, were milled for 5 min, and followed by 2 min pause for 24 repeated sequences, using a speed of 350 rpm and a total milling time of 120 minutes. Minor amounts of WC is observed in some of the samples. All preparations and manipulations of the samples were performed in an argon-filled glove box with a circulation purifier, $p(O_2, H_2O)$ < 1 ppm. All samples are labelled according to the molar fraction of $LiBH_4$, *e.g.* s2 (20 mol%) and s9.5 (95 mol%), an overview is provided in Table 1.

Table 1 Overview of produced samples and characterizations. HT-PXD = high-temperature powder X-ray diffraction; TPPA = temperature-programmed photographic analysis; DSC = differential scanning calorimetry; SR-PXD = synchrotron radiation powder X-ray diffraction

Sample	$LiBH_4$[a] (% mol)	Characterization
$NaBH_4$	0	HT-PXD
s1	10	TPPA, DSC, SR-PXD, HT-PXD
s2	20	TPPA, DSC, SR-PXD
s3	30	TPPA, DSC, HT-PXD
s4	40	TPPA, DSC
s5	50	TPPA, DSC, SR-PXD
s6	60	TPPA, DSC
s6.2	62	TPPA, DSC
s6.5	65	TPPA, DSC
s7	70	TPPA, DSC, HT-PXD
s7.5	75	DSC
s8	80	TPPA, DSC, SR-PXD
s9	88	TPPA, DSC, SR-PXD, HT-PXD
s9.5	95	DSC
s9.8	98	DSC
$LiBH_4$	100	DSC, HT-PXD

[a] Synthetised by ball milling.

Characterization

High-temperature laboratory powder X-ray diffraction (HT-PXD). High-temperature powder X-ray diffraction (HT-PXD) measurements were performed using a Rigaku Smart Lab X-ray diffractometer with parallel beam multilayer mirror (Cu radiation, $\lambda = 1.54059$ Å). Data were collected at room temperature (RT), 80, 150 and 200 °C, between $2\theta = 10$–$70°$, at a speed of 3° per minute with an HyPix-3000 high-resolution/high-speed 2D photon counting X-ray detector.[29] Samples were mounted in the glove box in 0.8 mm borosilicate glass capillaries and sealed with plastiline, then moved out of the glove box and sealed with flame. In order to allow the reaction to reach equilibrium, samples were heated up to the selected temperatures and four patterns were collected during each isothermal annealing for a total isotherm time of 100 min.

***In situ* time-resolved synchrotron radiation powder X-ray diffraction (SR-PXD).** *In situ* SR-PXD experiments were conducted at the beam line I711 at the MAX-II, MAXLAB laboratories, Lund, Sweden, with a Titan CCD detector system,[30] at a selected wavelength of $\lambda = 0.9938$ Å with 30 s exposure time. The setup for *in situ* measurements was a sample cell specifically developed to study solid–gas reactions, applying a pressure or a heating ramp.[31] The samples were packed in a single-crystal sapphire tube (o.d. 1.09 mm, i.d. 0.79 mm) and mounted on the sample cell in the glove box. To guarantee an inert environment around the sample, graphite ferrules were used to tighten the sapphire tube. A hot air blower heated the sample from RT to 500 °C at $\Delta T/\Delta t = 5$ °C min^{-1} in an argon atmosphere; the temperature was recorded by a thermocouple. Both the blower and the thermocouple were connected to a programmable PID temperature controller and the temperature was calibrated using NaCl (NIST) as a standard. The raw 2D diffraction datasets collected were transformed to a 1D powder patterns with the FIT2D program and a mask was used to remove the undesired spots from the single-crystal sapphire tube and shadow from the sample holder.[32] All PXD data have been refined by the Rietveld method using the Fullprof program.[33]

Thermal analysis. Differential scanning calorimetry (DSC) data were obtained using a PerkinElmer STA 6000 apparatus. The samples (approx. 2.5 mg) were loaded into Al crucibles with a lid inside the glove box and closed with a press; a hole was made in the lid to allow gaseous decomposition products to be released. The sample was then placed in a sealed glass vial, transported to the instrument and quickly placed in the instrument under an argon flow of 40 mL per minute. Samples were heated and cooled in the temperature range from RT to 500 °C at $\Delta T/\Delta t = 5$ °C min^{-1}.

Temperature-programmed photographic analysis (TPPA). Temperature-programmed photographic analysis (TPPA) was performed by collecting photographs using a digital camera whilst heating the samples from RT to 400 °C at $\Delta T/\Delta t = 5$ °C min^{-1}, using a setup previously described.[16] Samples (approx. 10 mg) were pressed into a pellet inside the glove box and then loaded in a vial and sealed with a septum to keep the inert argon atmosphere. The vial was placed in an aluminium block with viewing windows for photography and a thermocouple was

placed on one side of the vial to measure the temperature of the sample. A rubber balloon filled with argon was connected to the sample holder, in order to keep an inert atmosphere and to maintain the pressure constant in the case of release of gas.

Modelling

Ab initio. The calculations were performed using the periodic quantum-mechanical software CRYSTAL14 [34,35] within the Density Functional Theory. We have tested both GGA (PBE[36]) and hybrid (PBE0,[37] B3LYP[38,39]) functionals, with and without Grimme's D2 correction to the electronic energy.[40] We chose the PBE0-D2 level of theory, as the best compromise in terms of accuracy and cost of the calculations. The CRYSTAL code utilizes localized Gaussian functions to describe electrons. In detail: lithium cation was described with a 5-11G(d) basis set ($\alpha_{sp} = 0.479$ bohr^{-2} for the most diffuse shell exponent and $\alpha_{pol} = 0.600$ bohr^{-2} for polarization); sodium cation with a 8-511G ($\alpha_{sp} = 0.323$ bohr^{-2} for the most diffuse shell exponent), while for boron a 6-21G(d) was adopted ($\alpha_{sp} = 0.124$ bohr^{-2} for the most diffuse shell exponent and $\alpha_{pol} = 0.800$ bohr^{-2} for polarization) and for hydrogen, a 31G(p) ($\alpha_{sp} = 0.1613$ bohr^{-2} for the most diffuse shell exponent and $\alpha_{pol} = 1.1$ bohr^{-2} for polarization) was considered.[41] Phonons at Γ point in the harmonic approximation were computed to derive the thermodynamic functions by diagonalizing the associated mass-weighted Hessian matrix (for details on the computational procedure see references).[42,43] Enthalpy data were obtained by computing the electronic energy, inclusive of the zero-point energy correction (ZPE), and the thermal factor at $T = 25$ °C.[23]

Calphad. The Thermo-Calc Software[44] was used for the thermodynamic calculations. The Substance SGTE database[45,46] and already published thermodynamic functions[47] were used as a starting point for the thermodynamic assessment, providing thermodynamic functions for stable stoichiometric compounds. New thermodynamic functions for four $LiBH_4$–$NaBH_4$ solution phases (hexagonal, cubic, orthorhombic and liquid) have been evaluated in the present work.

According to the calphad approach, the Gibbs free energy of $LiBH_4$–$NaBH_4$ solution phases has been expressed as:[28]

$$^{\varphi}G = {}^{\varphi}G^{ref} - TS^{id} + {}^{\varphi}G^{exc} \quad (1)$$

$$^{\varphi}G^{ref} = x\,{}^{\varphi}G(LiBH_4) + (1 - x)\,{}^{\varphi}G(NaBH_4) \quad (2)$$

$$S^{id} = -R[x\ln(x) + (1 - x)\ln(1 - x)] \quad (3)$$

where φ is the considered phase, x is the molar fraction of $LiBH_4$, T is the temperature and G^{ref}, TS^{id} and G^{exc} are the reference, ideal entropy and the excess contributions to the Gibbs energy, respectively. Excess Gibbs energy was modelled with a Redlich–Kister expansion series[48] truncated to the second contribution or before, if the agreement with thermodynamic data was satisfactory:

$$^{\varphi}G^{exc} = x(1 - x)(^{1}a + {}^{1}bT) + x(1 - x)(2x - 1)(^{2}a + {}^{2}bT) \quad (4)$$

where ^{1}a, ^{1}b, ^{2}a and ^{2}b are optimized parameters.

Thermodynamic functions for missing end-members (*i.e.* ortho- and hexagonal-$NaBH_4$ and cubic-$LiBH_4$) were evaluated adding to the Gibbs energy of the stable phase the *ab initio* calculated enthalpy difference between the stable and the metastable structures.

Results and discussion

Eutectic melting of $LiBH_4$–$NaBH_4$

The DSC traces, corresponding onset temperatures and peak's area of phase transformation are reported in ESI† for all investigated compositions (Table S2, Fig. S2†) and the results of sample s7, s9.5 and 9.8 are reported in Fig. 1. Pure $LiBH_4$ is known to undergo a polymorphic transition from an orthorhombic (o) phase to a hexagonal (h) phase at about 108 °C and to melt at 280 °C.[16,47] Pure $NaBH_4$ is reported to melt at 505 °C.[16,49,50]

In the thermal analysis of the studied mixtures, three main events can be distinguished: polymorphic transition, eutectic melting and complete melting. An endothermic DSC peak associated to the polymorphic transition from o-$LiBH_4$ to h-$LiBH_4$ was observed during heating at 94 °C and during cooling at 85 °C. A change in the polymorphic transition temperature, with respect to that observed for pure $LiBH_4$, implies the formation of both orthorhombic and hexagonal

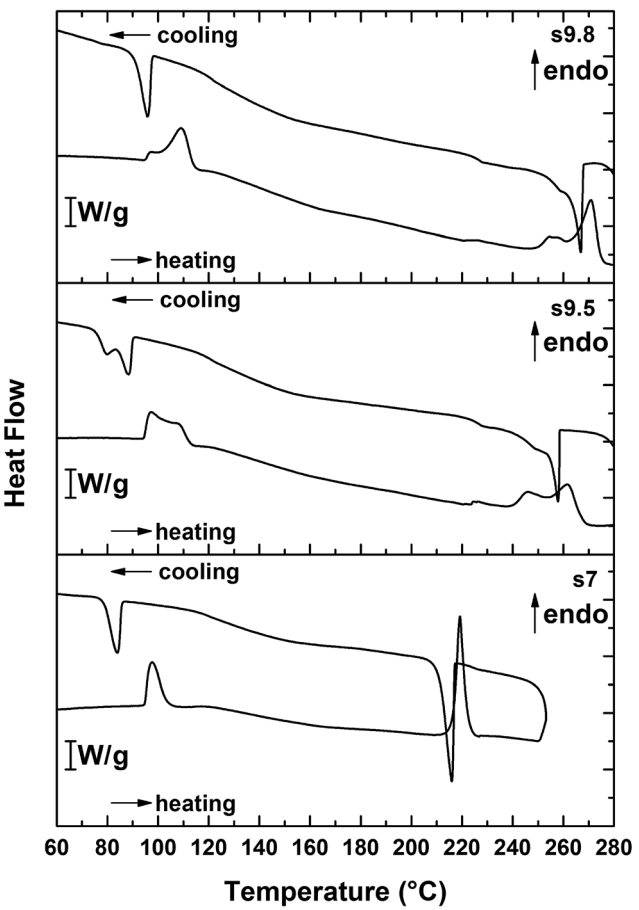

Fig. 1 DSC traces of s7, s9.5 and s9.8 on heating and cooling ($\Delta T/\Delta t = 5$ °C min^{-1}, 40 mL per minute argon flow).

solid solutions, dissolution of $NaBH_4$ into o-$LiBH_4$ structure-stabilized h-$LiBH_4$ and lowered the polymorphic transition temperature; a higher solubility of sodium is expected in the hexagonal phase with respect to the orthorhombic one. The eutectic melting is observed at 216 °C and, in samples that do not decompose or melt at too high temperature, another endothermic peak, corresponding to the complete melting was recorded in the DSC measurements (Fig. S2†). This peak was usually better observed during cooling, so that the onset liquidus temperature could be evaluated. A single melting peak is recorded at 216 °C for s7 (Fig. 1), suggesting a eutectic composition close to 70 mol% of $LiBH_4$. The area of DSC peak corresponding to the eutectic melting is also at the maximum for this composition (data reported in ESI, Table S2 and Fig. S2†), confirming the occurrence of eutectic melting.[14,15,51]

Selected pictures from TPPA for s2, s3, s6 and s7 are shown in Fig. 2. Measurements performed between room temperature and 400 °C confirm the results obtained from DSC analysis, showing a complete melting into a transparent liquid for the lithium-rich mixtures (s6–s9) starting from 220 °C (Fig. S1†).

Solid solutions

The DSC data indicates the formation of solid solutions and allows estimating the limit of solubility. In s9.8, a double endothermic peak is observed at low temperatures on heating (Fig. 1). The first peak corresponds to the complete solubility of $NaBH_4$ in the orthorhombic solid solution (solvus line). It shows a low intensity and starts at 94 °C, likely overheated with respect to the equilibrium temperature because of a solid-state dissolution. The second peak shows the o-to-h polymorphic transition, starting around 100 °C with an higher intensity. On cooling, only the h-to-o polymorphic transition is evidenced at 97 °C, likely in undercooling conditions. For sample s9.5 (Fig. 1), two overlapping endothermic peaks were also observed on heating in the same temperature range. Here, the intensity of the first peak is the highest, suggesting at first the occurrence of the polymorphic transition, followed by the formation of a single hexagonal phase. In the same sample, a double DSC peak was also observed on cooling, starting at 90 °C, corresponding to the same phase transitions in undercooling conditions. For samples containing less $LiBH_4$, *i.e.* from samples s6 to s9, a shoulder in main DSC peak was observed on heating (data reported in ESI†). It can be explained by a limited diffusion of $NaBH_4$ at such low temperatures, leading to a slow homogenization of the solid solution after o-to-h polymorphic transition. The different temperatures of the DCS peak recorded on cooling in sample s9, s9.5 and s9.8 suggest a solubility limit of sodium in the orthorhombic solid solution of *ca.* 5 mol%.

In order to study the structure of the solid solutions *in situ* SR-PXD measurements were performed on samples s1, s2, s5, s8 and s9. Exemplary, results for s9 are shown in Fig. 3, where polymorphic transition, eutectic and complete melting can be distinguished. At RT, the presence of $LiBH_4$ and $NaBH_4$ is observed in all samples. During heating in s8 (Fig. S6†) and s9 (Fig. 3), the

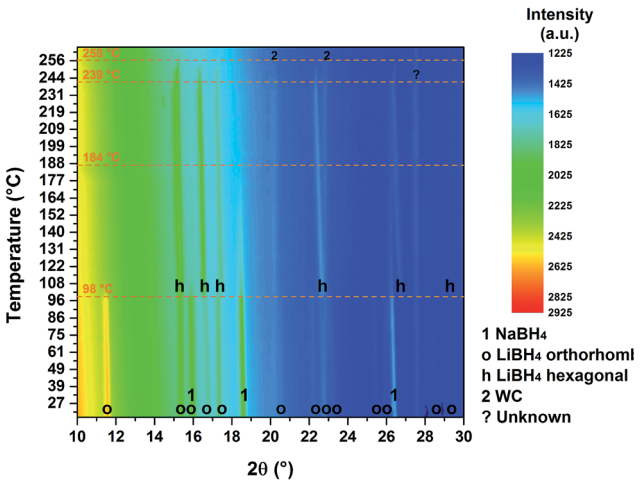

Fig. 3 *In situ* SR-PXD data for s9 ($\Delta T/\Delta t$ = 5 °C min^{-1}, argon atmosphere, temperature range 25–265 °C, λ = 0.9938 Å).

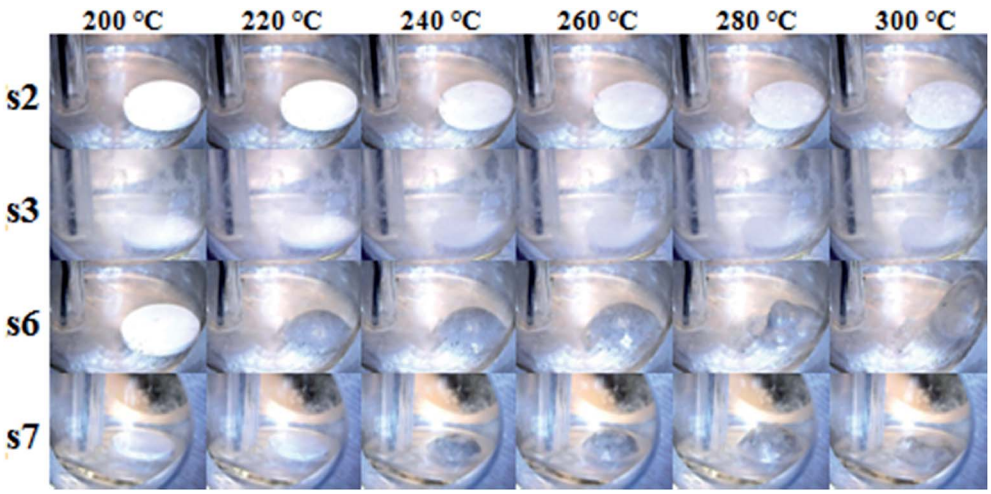

Fig. 2 Temperature-programmed photographic analysis (TPPA) of s2, s3, s6 and s7 ($\Delta T/\Delta t$ = 5 °C min^{-1}, argon atmosphere, temperature range 200–300 °C argon atmosphere).

reflections of $NaBH_4$ vanish at 211 °C and 184 °C, respectively, *i.e.* significantly below the melting temperature observed for the eutectic composition, recorded at 229 °C in s5. This indicates that the limit of solubility of $NaBH_4$ into the hexagonal solid solution cannot be lower than 20 mol%. Upon further heating, a release of $NaBH_4$ from the solid solution is observed in samples s8 from 232 °C and s9 from 239 °C, just before the complete melting at 248 °C and 258 °C, respectively. Due to a reduced solubility during the melting of the mixture, release of $NaBH_4$ from the hexagonal structure is observed by a shift at higher angles of the hexagonal reflections since the volume and cell parameter are reduced (Fig. 3 and S6†). There was no evidence of the formation of an orthorhombic solid solution from the PXD data, even if the lowered temperature upon heating of the polymorphic transition observed by DSC (Fig. 1) suggests its formation. It cannot be easily detected by PXD due to the low value of solubility of $NaBH_4$ into $LiBH_4$ (5%) and to possible overlapping of thermal expansion effects.

Also in samples rich in $NaBH_4$, the cubic solid solution cannot be identified, due to the low X-ray scattering power of lithium, so that the observed small shift of PXD reflections can be fully explained by thermal expansion.

Since the samples were synthesised by ball milling, in some cases traces of WC were observed by PXD (Fig. 3, S5 and S6†). WC is relatively inert and it is unlikely to influence any phase transformations nor its temperature. The deviation from literature values, in particular from ref. 17, cannot be related to the purity of the material, since the values recorded in our experimental study are significantly different.

Time-resolved *in situ* SR-PXD was conducted with constant heating measurements and does not probe the formation of a solid solution in equilibrium conditions. HT-PXD data were therefore collected for samples s1, s3, s7, s9 and pure ball-milled starting materials at various temperatures (22, 80, 150 and 200 °C) after heating and an isothermal annealing of 100 minutes (data reported in ESI†).

PXD analysis of starting materials confirmed a high purity, since no reflections from impurities are observed (Fig. S7 and S12†). The lattice constants of $LiBH_4$ and $NaBH_4$ were obtained from the Rietveld refinement of the HT-PXD data and the unit cell volume is plotted in Fig. 4 as a function of temperature.

At 22 and 80 °C, orthorhombic $LiBH_4$ is present, while at 150 and 200 °C, the hexagonal polymorph was observed (Fig. S12 in ESI†). For samples containing $NaBH_4$, the unit cell volume of the orthorhombic structure is rather similar at 80 °C (Fig. 4A), confirming that only a small amount of $NaBH_4$ can be accommodated. Since in sample s9 reflections of $NaBH_4$ are still present at 80 °C (Fig. S11 in ESI†), the limit of solubility has to be lower than 10 mol%, confirming the value (5 mol%) observed from DSC analysis (Fig. 1). The refined unit cell volume of the hexagonal phase is larger in samples containing $NaBH_4$ with respect to pure $LiBH_4$ at 150 and 200 °C (Fig. 4A), indicating that a solid solution is formed. In sample s9, at 150 °C, all $NaBH_4$ has dissolved into the hexagonal solid solution (Fig. S11 in ESI†), whereas it is still present in sample s7 at the same temperature (Fig. S10 in ESI†). So, the limit of solubility of $NaBH_4$ in the hexagonal solid solution can be estimated to lie between 10 mol% and 30 mol%.

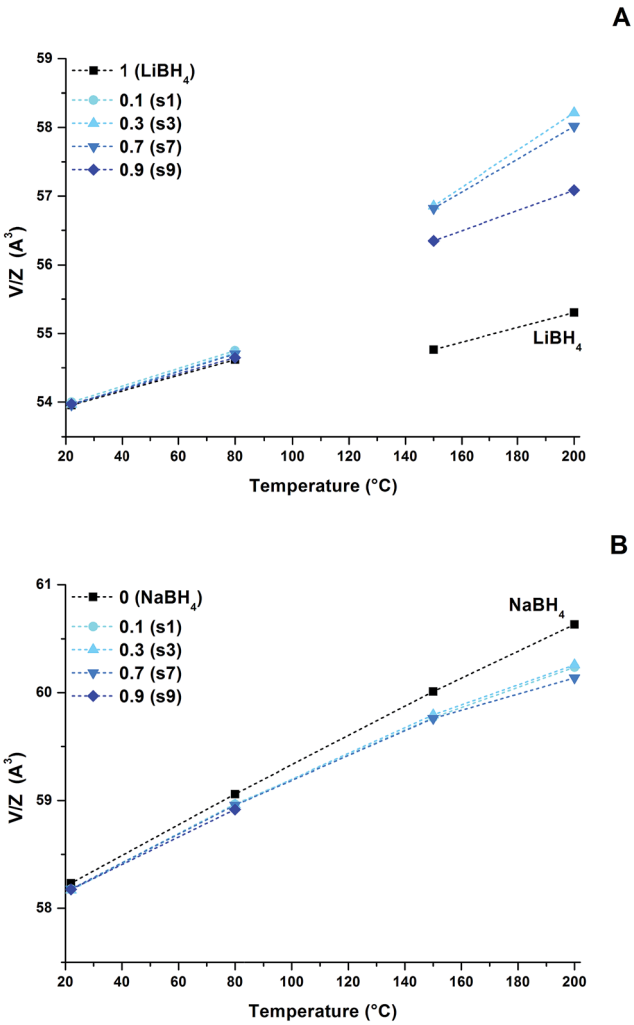

Fig. 4 Unit cell volume as a function of temperature for samples s1, s3, s7 and s9. Results from refinement of orthorhombic and hexagonal solid solutions (A), and the cubic solid solution (B). Dashed line is a guide for the eyes.

The refinement of PXD data of pure $NaBH_4$ (Fig. S7 in ESI†) provided information on the linear thermal expansion of the compound ($\alpha = 4.7 \times 10^{-4}$ K^{-1} in the temperature range 25–200 °C), as shown in Fig. 4B, in good agreement with the literature value ($\alpha = 5.36(6) \times 10^{-4}$ K^{-1} in the temperature range 46–200 °C).[21] In sample s1, the XRD peaks of $LiBH_4$ disappear at 150 °C (Fig. S8 in ESI†), indicating a complete solubility of 10 mol% of lithium in the cubic solid solution. In all samples containing $LiBH_4$, the unit cell volume is smaller (Fig. 4B), confirming the formation of a cubic solid solution. Since the unit cell volume for sample s1, s3 and s7 is very similar, the maximum solubility of $LiBH_4$ into $NaBH_4$ can be estimated close to 10 mol%.

Thermodynamic modelling and $LiBH_4$–$NaBH_4$ pseudo-binary phase diagram

Ab initio calculations were performed in order to obtain the lattice stabilities for the various structures, *i.e.* the difference in enthalpy (ΔH) with respect to the stable one, for both $LiBH_4$ and

$NaBH_4$. This evaluation is indeed essential to perform the thermodynamic assessment of the system. Precisely, six structures were optimized, that is the cubic, orthorhombic and hexagonal phases for both borohydrides. The best optimization procedure, leading to energy minimum structures, as confirmed by the frequencies calculation (no imaginary modes), consisted of constrained symmetrized unit cell deformations. Thus, all the internal coordinates were fully relaxed maintaining the original lattice symmetry of the system. Computed results of ΔH at 25 °C, reported in Table 2, confirmed the relative stability of the experimentally observed polymorphs, (*i.e.* for $LiBH_4$: orthorhombic ≫ hexagonal > cubic and for the $NaBH_4$: cubic ≫ orthorhombic > hexagonal) and provided relevant data for the assessment of the phase diagram within the calphad scheme.

Experimental and literature data were critically compared and used for the assessment of the interaction parameters for the various solution phases (solid and liquid). Experimental information from ref. 17 was used for the assessment but, since data above polymorphic transition from ref. 18 were not clearly described and are significantly different from those obtained experimentally for all mixtures, they were not considered. In order to fit both the transition temperatures and the enthalpy of melting for the eutectic composition, the liquid phase was described using three interaction parameters. In fact, considering ^1a, ^2a and ^1b parameters in eqn (4), a value equal to 219 °C and 7.07 kJ mol^{-1} has been obtained, respectively, for the temperature and the enthalpy of melting, in good agreement with the experimental value of 216 °C and 6.99 kJ mol^{-1} from DSC data of sample s7. For solid solutions, an ideal or regular solution model was sufficient to describe the experimental data. The assessed thermodynamic parameters are reported in Table 2.

Calculated equilibrium lines and experimental points for the polymorphic transition, solubility limits, eutectic and liquidus temperatures are compared in Fig. 5. The experimental data reported for the polymorphic transition were obtained by DSC during heating and cooling and by SR-PXD during heating. The eutectic temperature was recorded by TPPA during heating, DSC during heating and cooling and SR-PXD during heating, while the liquidus temperature was recorded by DSC during cooling and SR-PXD during heating. In Fig. 5 also the solvus temperature obtained by SR-PXD and HT-PXD is reported. The eutectic point is calculated at 71 mol% of $LiBH_4$ and 219 °C. The calculated temperature for the polymorphic transition from orthorhombic-to-hexagonal is 97 °C, in good agreement with the results reported on Fig. 1. The calculated limit of solubility of $LiBH_4$ in the cubic solid solution is 7 mol%. The calculated solubility limit of $NaBH_4$ is 6 mol% and 20 mol% into the orthorhombic and hexagonal solid solutions, respectively, in agreement with X-ray diffraction results.

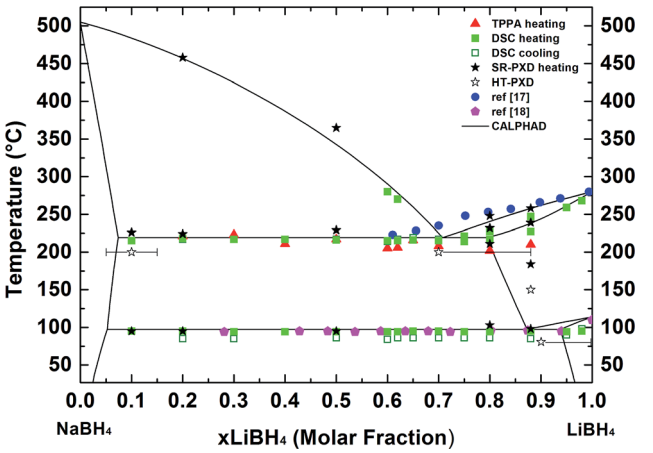

Fig. 5 Pseudo-binary phase diagram of the $LiBH_4$–$NaBH_4$ system. Experimental and literature data (points) are compared with the calculation (lines) from the calphad assessment.

Table 2 List of models and optimized parameters obtained from the assessment of the pseudo-binary system

Gibbs free energy (J mol^{-1})	Model
$^{CUB}G(LiBH_4) = G(LiBH_4) + 3600$	
$^{ORT}G(NaBH_4) = G(NaBH_4) + 8400$	
$^{HEX}G(NaBH_4) = G(NaBH_4) + 6200$	
$^{CUB}G^{exc} = x(1-x)\ (5887)$	Regular
$^{ORT}G^{exc} = 0$	Ideal
$^{HEX}G^{exc} = 0$	Ideal
$^{LIQ}G^{exc} = x(1-x)(-20063 + 23T) + x(1-x)(2x-1)\ (2542)$	RK

In general, solubility in the system $LiBH_4$–$NaBH_4$ may depend on the crystal structure and the relative cationic sizes, which are $r(Li^+) = 0.76$ Å and $r(Na^+) = 1.02$ Å. The volume per formula unit at 110 °C is similar for cubic $NaBH_4$, orthorhombic and hexagonal $LiBH_4$: $V/Z(NaBH_4) = 59.44$ Å^3, V/Z(o-$LiBH_4$) = 54.96 Å^3 and V/Z(h-$LiBH_4$) = 54.33 Å^3.

From a thermodynamic point of view, the solubility limit is affected by two main contributions: the enthalpy of mixing and the difference in lattice stability between the stable and the metastable structure of the pure compounds (end-members) as previously reported in another study.[52] In this study, the lattice stability of o-$NaBH_4$, h-$NaBH_4$ and c-$LiBH_4$ (Table 2) were determined from *ab initio* calculations and an enthalpy of mixing equal to zero, as well as an ideal entropy, were assumed for both orthorhombic and hexagonal solid solutions. In fact, high solubility limit can be obtained if the difference in energy between stable and metastable structures of the end member is low. A high limit of solubility of sodium in the hexagonal structure of lithium borohydride can then be reached because the free energy of $NaBH_4$ in the hexagonal structure is slightly higher than that of the cubic structure. Furthermore, because the free energy of $NaBH_4$ in the orthorhombic structure is much higher, the solubility turns out more limited.

The solubility of $NaBH_4$ in h-$LiBH_4$ is significantly stronger as compared to o-$LiBH_4$. This suggest that other phenomena, *e.g.* dynamic or entropy effects may be important.

Previous work on anion substitution in metal borohydrides clearly show that limited amounts of alkali metal halides can dissolve in orthorhombic room temperature polymorph of lithium borohydride, o-$LiBH_4$, but these salts readily dissolve in the hexagonal polymorph, h-$LiBH_4$.[19,20,24,53,54]

Neutron diffraction and solid state MAS NMR suggest that there is significant higher degree of dynamics in h-$LiBH_4$ as compared to o-$LiBH_4$.[20,55] These dynamic or entropy effects strongly influence cation jump frequency, *i.e.* the ion conductivity, which is higher in h-$LiBH_4$ as compared to o-$LiBH_4$.[25,27] Thus, the increased cation dynamics in h-$LiBH_4$ may contribute to increased solubility of $NaBH_4$ in h-$LiBH_4$ as observed experimentally in this study. Therefore, an entropy effect may contribute to the increased solubility of $NaBH_4$ in h-$LiBH_4$. Nevertheless, dynamic effects in the solid state are challenging to quantify experimentally and therefore the orthorhombic and hexagonal solid solutions has been assumed ideal in this study, *i.e.* enthalpy of mixing equal to zero, $\Delta H_{mix} = 0$.

The knowledge of thermodynamic properties of binary system as a function of composition and temperature is of fundamental importance for tailoring the mechanism of hydrogen release and uptake reactions. The formation of solid solutions and the determination of their enthalpies of mixing allow to tailor the enthalpy of dehydrogenation towards values around 35 kJ mol^{-1} H_2, which are necessary for a hydrogen release and uptake at ambient condition (*i.e.* room temperature and $p(H_2) = 1$ bar).[52]

Dynamic effects in the solid state may be important in order to tailor transport phenomena like hydrogen release and uptake and ion conductivity. The formation of substitutional solid solutions, which stabilizes the hexagonal high temperature polymorph, h-$LiBH_4$, at lower temperatures may allow to utilize dynamic or entropy effects. Many studies has been performed on anion substitution to stabilize the hexagonal polymorph to room temperature, but cation substitution is less explored for improving hydrogen storage properties[56] and ion conductivity for metal borohydrides and *closo*-boranes.[57,58] Further investigations are necessary to study systematically the influence of cation solid solution on ionic conduction in borohydrides.

Conclusions

A thermodynamic investigation of the $LiBH_4$–$NaBH_4$ system has been carried out, combining experimental data, *ab initio* calculations and thermodynamic modelling. Enthalpy differences among the stable and metastable phases of the end-members were computed by means of *ab initio* calculations, using the CRYSTAL14 code. These data were considered within the calphad approach to calculate the phase diagram, obtaining a good agreement between predicted values and experimental ones. According to thermodynamic modelling, the eutectic point was determined to be at 71 $LiBH_4$ mol% and 219 °C, in good agreement with results of DSC, *in situ* SR-PXD and temperature-programmed photographic analysis. Thermal analysis indicates the existence of an orthorhombic solid solution with a solubility of sodium in $LiBH_4$ higher than 5 mol%, as confirmed by calphad calculations, which predicted a phase transition temperature at 97 °C with a 6 mol% maximum dissolution of sodium in the orthorhombic phase. *In situ* SR-PXD data and HT-PXD allowed identifying a hexagonal solid solution at temperatures above the polymorphic transition, with a limit of solubility of sodium in between 10 mol% and 30 mol%, corresponding well to a maximum solubility of 20 mol% $NaBH_4$ calculated from calphad. HT-PXD also showed the formation of a cubic solid solution, with a limit of solubility of Li close 10 mol%, corresponding to a value of 7 mol% $LiBH_4$ calculated from calphad.

Acknowledgements

Financial support from the European Fuel Cells and Hydrogen Joint Undertaking in the framework of the BOR4STORE (Grant agreement no. 303428) is thankfully acknowledged. The work was supported by The Innovation Fund Denmark, *via* the research project HyFillFast, the Danish National Research Foundation, Center for Materials Crystallography (DNRF93), and by the Danish Research Council for Nature and Universe (Danscatt). The access to beamtime at the MAX-II synchrotron, Lund, Sweden in the MAXIV research laboratory is gratefully acknowledged.

References

1 Q. Lai, M. Paskevicius, D. A. Sheppard, C. E. Buckley, A. W. Thornton, M. R. Hill, Q. Gu, J. Mao, Z. Huang, H. K. Liu, Z. Guo, A. Banerjee, S. Chakraborty, R. Ahuja and K. F. Aguey Zinsou, *ChemSusChem*, 2015, **8**, 2789–2825.
2 M. B. Ley, L. H. Jepsen, Y.-S. Lee, Y. W. Cho, J. M. Bellosta von Colbe, M. Dornheim, M. Rokni, J. O. Jensen, M. Sloth, Y. Filinchuk, J. E. Jørgensen, F. Besenbacher and T. R. Jensen, *Mater. Today*, 2014, **17**, 122–128.
3 L. H. Jepsen, M. B. Ley, Y. S. Lee, Y. W. Cho, M. Dornheim, J. O. Jensen, Y. Filinchuk, J. E. Jørgensen, F. Besenbacher and T. R. Jensen, *Mater. Today*, 2014, **17**, 129–135.
4 H. W. Li, Y. Yan, S. I. Orimo, A. Züttel and C. M. Jensen, *Energies*, 2011, **4**, 185–214.
5 E. Callini, Z. Ö. K. Atakli, B. C. Hauback, S. Orimo, C. Jensen, M. Dornheim, D. Grant, Y. W. Cho, P. Chen, B. Hjörvarsson, P. de Jongh, C. Weidenthaler, M. Baricco, M. Paskevicius, T. R. Jensen, M. E. Bowden, T. S. Autrey and A. Züttel, *Appl. Phys. A*, 2016, **122**, 353.
6 K. Takahashi, K. Hattori, T. Yamazaki, K. Takada, M. Matsuo, S. I. Orimo, H. Maekawa and H. Takamura, *J. Power Sources*, 2013, **226**, 61–64.
7 M. Matsuo and S. I. Orimo, *Adv. Energy Mater.*, 2011, **1**, 161–172.
8 M. Matsuo, A. Remhof, P. Martelli, R. Caputo, M. Ernst, Y. Miura, T. Sato, H. Oguchi, H. Maekawa, H. Takamura, A. Borgschulte, A. Züttel and S. I. Orimo, *J. Am. Chem. Soc.*, 2009, **131**, 16389–16391.
9 E. Roedern, B. R. S. Hansen, M. B. Ley and T. R. Jensen, *J. Phys. Chem. C*, 2015, **119**, 25818–25825.
10 P. Javadian and T. R. Jensen, *Int. J. Hydrogen Energy*, 2014, **39**, 9871–9876.
11 A. Doroodian, J. E. Dengler, A. Genest, N. Rösch and B. Rieger, *Angew. Chem., Int. Ed.*, 2010, **49**, 1871–1873.
12 S. Li, H. Gao and J. M. Shreeve, *Angew. Chem., Int. Ed.*, 2014, **53**, 2969–2972.

13 H. W. Li, S. I. Orimo, Y. Nakamori, K. Miwa, N. Ohba, S. I. Towata and A. Züttel, *J. Alloys Compd.*, 2007, **446–447**, 315–318.
14 M. B. Ley, E. Roedern and T. R. Jensen, *Phys. Chem. Chem. Phys.*, 2014, **16**, 24194–24199.
15 J. Y. Lee, D. B. Ravnsbæk, Y. S. Lee, Y. Kim, Y. Cerenius, J. Shim, T. R. Jensen, N. H. Hur and Y. W. Cho, *J. Phys. Chem. C*, 2009, **113**, 15080–15086.
16 M. Paskevicius, M. B. Ley, D. A. Sheppard, T. R. Jensen and C. E. Buckley, *Phys. Chem. Chem. Phys.*, 2013, **15**, 19774.
17 R. M. Adams, *Adv. Chem.*, 1961, **32**, 60–68.
18 K. N. Semenenko, A. P. Chavgun and V. N. Surov, *Russ. J. Inorg. Chem.*, 1971, **16**, 271–273.
19 O. Zavorotynska, M. Corno, E. R. Pinatel, L. H. Rude, P. Ugliengo, T. R. Jensen and M. Baricco, *Crystals*, 2012, **2**, 144–158.
20 L. M. Arnbjerg, D. B. Ravnsbæk, Y. Filinchuk, R. T. Vang, Y. Cerenius, F. Besenbacher, J.-E. Jørgensen, H. J. Jakobsen and T. R. Jensen, *Chem. Mater.*, 2009, **21**, 5772–5782.
21 D. B. Ravnsbæk, L. H. Rude and T. R. Jensen, *J. Solid State Chem.*, 2011, **184**, 1858–1866.
22 J. E. Olsen, P. Karen, M. H. Sørby and B. C. Hauback, *J. Alloys Compd.*, 2014, **587**, 374–379.
23 M. Corno, E. Pinatel, P. Ugliengo and M. Baricco, *J. Alloys Compd.*, 2011, **509**, S679–S683.
24 L. H. Rude, O. Zavorotynska, L. M. Arnbjerg, D. B. Ravnsbæk, R. A. Malmkjær, H. Grove, B. C. Hauback, M. Baricco, Y. Filinchuk, F. Besenbacher and T. R. Jensen, *Int. J. Hydrogen Energy*, 2011, **36**, 15664–15672.
25 A. V. Skripov, A. V. Soloninin, L. H. Rude, T. R. Jensen and Y. Filinchuk, *J. Phys. Chem. C*, 2012, **116**, 26177–26184.
26 R. Miyazaki, T. Karahashi, N. Kumatani, Y. Noda, M. Ando, H. Takamura, M. Matsuo, S. I. Orimo and H. Maekawa, *Solid State Ionics*, 2011, **192**, 143–147.
27 H. Maekawa, M. Matsuo, H. Takamura, M. Ando, Y. Noda, T. Karahashi and S. I. Orimo, *J. Am. Chem. Soc.*, 2009, **131**, 894–895.
28 H. L. Lukas, S. G. Fries and B. Sundman, *Computational thermodynamics, the calphad method*, 2007.
29 *Rigaku J.*, 2014, **30**(2), 38–40.
30 Y. Cerenius, K. Ståhl, L. A. Svensson, T. Ursby, Å. Oskarsson, J. Albertsson and A. Liljas, *J. Synchrotron Radiat.*, 2000, **7**, 203–208.
31 T. R. Jensen, T. K. Nielsen, Y. Filinchuk, J. E. Jørgensen, Y. Cerenius, E. M. Gray and C. J. Webb, *J. Appl. Crystallogr.*, 2010, **43**, 1456–1463.
32 A. P. Hammersley, S. O. Svensson, M. Hanfland, A. N. Fitch and D. Hausermann, *Adv. High Pressure Res.*, 1996, **14**, 235–248.
33 J. Rodriguez-Carvajal, *Fullprof Suite: LLB Sacley & LCSIM Rennes*, 2003.
34 R. Dovesi, V. R. Saunders, C. Roetti, R. Orlando, C. M. Zicovich-Wilson, F. Pascale, B. Civalleri, K. Doll, N. M. Harrison, I. J. Bush, P. D'Arco, M. Llunell, M. Causà and Y. Noël, *CRYSTAL14 User's Manual*, University of Torino, 2014.
35 R. Dovesi, R. Orlando, A. Erba, C. M. Zicovich-Wilson, B. Civalleri, S. Casassa, L. Maschio, M. Ferrabone, M. De La Pierre, P. D'Arco, Y. Noël, M. Causà, M. Rérat and B. Kirtman, *Int. J. Quantum Chem.*, 2014, **114**, 1287–1317.
36 J. P. Perdew, K. Burke and M. Ernzerhof, *Phys. Rev. Lett.*, 1996, **77**, 3865–3868.
37 C. Adamo and V. Barone, *J. Chem. Phys.*, 1999, **110**, 6158.
38 C. Lee, W. Yang and R. G. Parr, *Phys. Rev. B: Condens. Matter Mater. Phys.*, 1988, **37**, 785–789.
39 A. D. Becke, *J. Chem. Phys.*, 1993, **98**, 5648.
40 S. Grimme, *J. Comput. Chem.*, 2006, **27**, 1787–1799.
41 O. Zavorotynska, M. Corno, A. Damin, G. Spoto, P. Ugliengo and M. Baricco, *J. Phys. Chem. C*, 2011, **115**, 18890–18900.
42 F. Pascale, C. M. Zicovich-Wilson, F. Lopez Gejo, B. Civalleri, R. Orlando and R. Dovesi, *J. Comput. Chem.*, 2004, **25**, 888–897.
43 C. M. Zicovich-Wilson, F. J. Torres, F. Pascale, L. Valenzano, R. Orlando and R. Dovesi, *J. Comput. Chem.*, 2008, **29**, 2268–2278.
44 J. O. Andersson, T. Helander, L. Hoglund, P. Shi and B. Sundman, *Calphad*, 2002, **26**, 273–312.
45 A. T. Dinsdale, *Calphad*, 1991, **15**, 317–425.
46 *SGTE substance database V 4.1*, http://www.crct.polymtl.ca/fact/documentation/sgps_list.htm.
47 A. El Kharbachi, E. Pinatel, I. Nuta and M. Baricco, *Calphad*, 2012, **39**, 80–90.
48 A. T. Kister and O. Redlich, *Ind. Eng. Chem.*, 1948, **40**, 345–348.
49 J. Urgnani, F. J. Torres, M. Palumbo and M. Baricco, *Int. J. Hydrogen Energy*, 2008, **33**, 3111–3115.
50 P. Martelli, R. Caputo, A. Remhof, P. Mauron, A. Borgschulte and A. Züttel, *J. Phys. Chem. C*, 2010, **114**, 7173–7177.
51 M. Ley, E. Roedern, P. Thygesen and T. R. Jensen, *Energies*, 2015, **8**, 2701–2713.
52 E. R. Pinatel, M. Corno, P. Ugliengo and M. Baricco, *J. Alloys Compd.*, 2014, **615**, S706–S710.
53 L. Mosegaard, B. Moller, J. E. Jørgensen, Y. Filinchuk, Y. Cerenius, J. C. Hanson, E. Dimasi, F. Besenbacher and T. R. Jensen, *J. Phys. Chem. C*, 2008, **112**, 1299–1303.
54 L. H. Rude, E. Groppo, L. M. Arnbjerg, D. B. Ravnsbæk, R. A. Malmkjær, Y. Filinchuk, M. Baricco, F. Besenbacher and T. R. Jensen, *J. Alloys Compd.*, 2011, **509**, 8299–8305.
55 M. R. Hartman, J. J. Rush, T. J. Udovic, R. C. Bowman and S.-J. Hwang, *J. Solid State Chem.*, 2007, **180**, 1298–1305.
56 G. N. Kalantzopoulos, J. G. Vitillo, E. Albanese, E. R. Pinatel, B. Civalleri, S. Deledda, S. Bordiga, M. Baricco and B. C. Hauback, *J. Alloys Compd.*, 2014, 10–13.
57 W. S. Tang, T. J. Udovic and V. Stavila, *J. Alloys Compd.*, 2015, **645**, S200–S204.
58 Y. Sadikin, M. Brighi, P. Schouwink and R. Černý, *Adv. Energy Mater.*, 2015, **5**, 1–6.

